Eidgenössische Technische Hochschule Zürich

Ecole polytechnique fédérale de Zurich
Politecnico federale di Zurigo
Swiss Federal Institute of Technology Zurich

Sparse tensor spherical harmonics approximation in radiative transfer*

K. Grella and Ch. Schwab

Research Report No. 2010-33
October 2010

Seminar für Angewandte Mathematik
Eidgenössische Technische Hochschule
CH-8092 Zürich
Switzerland

*Partial support by the Swiss National Science Foundation (SNF) under Project no. 121892 and by ERC AdG no. 247277 STAHDPDE is acknowledged.

Sparse Tensor Spherical Harmonics Approximation in Radiative Transfer*

K. Grella, Ch. Schwab
Seminar für Angewandte Mathematik
Eidgenössische Technische Hochschule
CH-8092 Zürich
Switzerland

October 13, 2010

The stationary monochromatic radiative transfer equation is a partial differential transport equation stated on a five-dimensional phase space. To obtain a well-posed problem, inflow boundary conditions have to be prescribed.

The sparse tensor product discretization has been successfully applied to finite element methods in radiative transfer with wavelet discretization of the angular domain (Widmer 2009). In this report we show that the sparse tensor product discretization can be combined with a spectral discretization of the angular domain using spherical harmonics.

Neglecting boundary conditions, we prove that the convergence rate of our method in terms of number of degrees of freedom is essentially the same as the convergence of the full tensor product method up to a logarithmic factor. For the case with boundary conditions, we propose a splitting of the physical function space and a conforming tensorization. Numerical experiments in two physical and one angular dimension show evidence for the theoretical convergence rates to hold in the latter case as well.

*Partial support by the Swiss National Science Foundation (SNF) under project no. 121892 and by ERC AdG no. 247277 STAHDPDE is acknowledged.

1 Introduction

1.1 Radiative transfer

In this work we are going to address the numerical solution of the stationary monochromatic radiative transfer problem (see e. g. Modest 2003) without scattering defined on a bounded Lipschitz domain $D \subset \mathbb{R}^d$, where $d = 2, 3$.

We would like to find the radiative intensity $u(\mathbf{x}, \mathbf{s})$, $u : D \times \mathcal{S}^{d_S} \to \mathbb{R}$, $\mathcal{S}^{d_S}$ being the sphere with $d_\mathcal{S} = 1, 2$, that satisfies

$$\mathbf{s} \cdot \boldsymbol{\nabla}_x u(\mathbf{x}, \mathbf{s}) + \kappa(\mathbf{x}) u(\mathbf{x}, \mathbf{s}) = \kappa(\mathbf{x}) I_b(\mathbf{x}), \quad (\mathbf{x}, \mathbf{s}) \in D \times \mathcal{S}^{d_S} \tag{1a}$$

$$u(\mathbf{x}, \mathbf{s}) = g(\mathbf{x}, \mathbf{s}), \qquad \mathbf{x} \in \partial D,\ \mathbf{s} \cdot \mathbf{n}(\mathbf{x}) < 0\ . \tag{1b}$$

$\kappa \geq 0$ is the absorption coefficient, $I_b \geq 0$ the blackbody intensity, $g \geq 0$ the wall emission, and $\mathbf{n}(\mathbf{x})$ the outer unit normal on the boundary. In general, the problem formulation could include scattering terms (Modest 2003). However, in this paper we neglect scattering since the focus of the investigation lies on the discretization of Eq. (1). Furthermore, we assume "cold walls" so that $g = 0$.

An introduction to the topic radiative heat transfer is given by Modest (2003). Apart from Monte Carlo methods, standard solution approaches to the radiative transfer problem are the discrete ordinates method and the method of spherical harmonics. Frank (2007) gives an overview of these numerical methods for radiative transfer. State-of-the-art methods and applications are compiled by Kanschat et al. (2008).

In the discrete ordinate method or S_N-approximation, Eq. 1 is solved for N fixed directions spanning the full range in solid angle. The method is simple to implement and thus popular, but in order to capture very localized features of the solution in the $\mathbf{s}$-dependence a fine angular resolution is necessary. Also, the method suffers from so-called *ray effects*, in which the mesh structure of the discretization is reflected in the solution.

The method of spherical harmonics or P_N-approximation works by expanding the intensity into a truncated series of spherical harmonics in the solid angle, which leads to a coupled (or decoupled if scattering is ignored) system of PDEs in space. Often used are the P_1-approximation, in which (1) is reduced to a diffusion equation, and higher order approximations up to $N = 7$. Even higher orders are usually avoided because the mathematical complexity for general problems increases rapidly while the accuracy for non-smooth functions in the solid angle improves only slowly with the number of spherical harmonics. For smooth solutions, the spherical harmonics method exhibit spectral convergence, which makes them a popular and promising approach for radiative transfer problems where smoothness in the solution is expected.

The system of partial differential equations arising from the S_N- or P_N-approximation is eventually solved with finite differences or a finite element method. Manteuffel et al. (2000), for instance, discretize a least squares formulation with spherical harmonics in the solid angle and finite elements in space. Kanschat (1996) uses the discrete ordinate method with FE discretization and streamline diffusion stabilization in the physical domain D.

All these methods suffer from the "curse of dimension", the low rate of convergence in terms of number of degrees of freedom due to the high dimensionality of the radiative transfer problem which is stated in five dimensions for $(d, d_{\mathcal{S}}) = (3, 2)$. The accuracy of the solution doesn't scale in the same way as the computational complexity so that accurate discretizations quickly become prohibitively expensive.

For the spherical harmonics method, there exists a simplified P_N-approximation (e. g. Larsen et al. 2002) to reduce the workload while maintaining accuracy. Modest and Yang (2008) suggest a successive elimination of spherical harmonic tensors to reduce the number of simultaneous differential equations from $(N+1)^2$ to $N(N+1)/2$ in 3D.

Widmer et al. (2007) have developed a method to overcome the curse of dimension in the context of a wavelet discretization of the angular domain. In their sparse tensor product method, they discretize physical and angular domain with hierarchical and wavelet finite elements, respectively, and then select only the most relevant finite element product combinations to construct the search space for the solution. Provided that the absorption coefficient $\kappa(\mathbf{x})$ and blackbody intensity $I_b(\mathbf{x})$ are sufficiently smooth, their method achieves a log-linear complexity in the number of degrees of freedom while convergence rates deteriorate only by a logarithmic factor. Unlike some other methods for radiative transfer, their method does not require κ to be large.

In this paper we combine the sparse tensor product method with a spectral discretization involving spherical harmonics, as already suggested by Widmer et al. (2008), and show that the advantages of sparse tensorization carry over to a combination of hierarchical finite elements in physical space and spectral discretization in solid angle. This sparse tensor spherical harmonics method for radiative transfer makes it possible to include spherical harmonics of high order without incurring an excessive computational burden.

1.2 Structure of paper

The paper is organized as follows: In Section 2 we reformulate the radiative transfer problem (1) into a variational problem with a least-squares approach.

In Section 3 we describe our discretization of the variational problem. We apply a Galerkin ansatz to the variational problem and define our product combination basis functions of hierarchical linear functions in physical space and spherical harmonics as well as Legendre polynomials in angular space. We define the full and sparse tensor product search space without and with boundary conditions and derive and prove approximation properties for the case neglecting boundary conditions.

Section 4 underlines the analytical derivations with results from numerical experiments in which we compare the usual full tensor product method to the sparse tensor product method.

1.3 Acknowledgments

The authors wish to express their thanks to Prof. Ralf Hiptmair for many fruitful discussions and valuable comments and suggestions.

2 Variational problem

To transform the radiative transfer problem (1) into a variational problem, we follow Widmer et al. (2007) closely.

For the remainder of the paper, we consider the *simplified, stationary radiation transfer problem with homogeneous Dirichlet boundary data*:
Find the intensity $u(\mathbf{x}, \mathbf{s}) : D \times \mathcal{S}^{d_\mathcal{S}} \to \mathbb{R}$ such that

$$(\mathbf{s} \cdot \boldsymbol{\nabla}_x + \kappa(\mathbf{x}))\, u(\mathbf{x}, \mathbf{s}) = \kappa(\mathbf{x}) I_b(\mathbf{x}) \tag{2a}$$

$$u(\mathbf{x}, \mathbf{s}) = 0, \quad \mathbf{x} \in \Gamma_-(\mathbf{s}),\ \mathbf{s} \in \mathcal{S}^{d_\mathcal{S}}, \tag{2b}$$

where $\Gamma_-(\mathbf{s})$ denotes the inflow boundary defined by

$$\Gamma_-(\mathbf{s}) := \{\mathbf{x} \in \partial D : \mathbf{s} \cdot \mathbf{n}(\mathbf{x}) < 0\} \subset \partial D, \quad \mathbf{s} \in \mathcal{S}^{d_\mathcal{S}}. \tag{3}$$

For our experiments later on, we consider the problem in two spatial dimensions, i. e. the case $(d, d_\mathcal{S}) = (2, 1)$. The analysis in this paper is conducted more generally with the case $(d, d_\mathcal{S}) = (3, 2)$ also in mind, which is more relevant for applications.

When regarding $\mathbf{s}$ as a mere parameter, the radiative transfer equation (2a) reduces to a linear convection equation for the directed intensity $u(\cdot, \mathbf{s})$. It is well known that its standard, continuous Galerkin discretization is unstable (e. g. Johnson 1987). We use the stabilized variational formulation of (2a) proposed by Manteuffel et al. (2000).

We seek $u : D \times \mathcal{S}^{d_\mathcal{S}} \mapsto \mathbb{R}$ as the minimizer of the quadratic least squares functional

$$J(u) := \frac{1}{2} \left(\epsilon(\mathbf{s} \cdot \boldsymbol{\nabla}_x u + \kappa u - \kappa I_b), \mathbf{s} \cdot \boldsymbol{\nabla}_x u + \kappa u - \kappa I_b\right)_{L^2} , \tag{4}$$

where

$$\epsilon(\mathbf{x}) = \begin{cases} 1, & \kappa(\mathbf{x}) < \kappa_0, \\ \frac{1}{\kappa(\mathbf{x})}, & \kappa(\mathbf{x}) \geq \kappa_0 \end{cases} \tag{5}$$

with $\kappa_0 \approx 0.134$ (for details, see Widmer et al. 2007). In (4), we adopted the notation

$$(u, v)_{L^2} := (u, v)_{L^2(D \times \mathcal{S}^{d_\mathcal{S}})} = \int_D \int_{\mathcal{S}^{d_\mathcal{S}}} u\, v \, d\mathbf{s}\, d\mathbf{x} \tag{6}$$

and the associated L^2-norm will be denoted by $\|\cdot\|_{L^2(D \times \mathcal{S}^{d_\mathcal{S}})} = \|\cdot\|_{L^2}$.

For the proper statement of this minimization problem as well as of the FEM below, we define the Hilbert spaces

$$\mathcal{V} := \{u \in L^2(D \times \mathcal{S}^{d_\mathcal{S}}) :\ \mathbf{s} \cdot \boldsymbol{\nabla}_x u \in L^2(D \times \mathcal{S}^{d_\mathcal{S}})\} \tag{7}$$

and

$$\mathcal{V}_0 := \left\{u \in \mathcal{V};\ u = 0 \text{ on } \Gamma_-(\mathbf{s}),\ \mathbf{s} \in \mathcal{S}^{d_\mathcal{S}}\right\}. \tag{8}$$

We equip $\mathcal{V}$ in (7) with the norm $\|\cdot\|_S$, defined by

$$\|u\|_S^2 := \|\mathbf{s} \cdot \boldsymbol{\nabla}_x u\|_{L^2}^2 + \|u\|_{L^2}^2. \tag{9}$$

We now introduce the bilinear form

$$a(u,v) := (\epsilon \mathbf{s}\cdot\boldsymbol{\nabla}_x u, \mathbf{s}\cdot\boldsymbol{\nabla}_x v)_{L^2} + (\epsilon\mathbf{s}\cdot\boldsymbol{\nabla}_x u, \kappa v)_{L^2} + (\epsilon\kappa u, \mathbf{s}\cdot\boldsymbol{\nabla}_x v)_{L^2} + (\epsilon\kappa u, \kappa v)_{L^2} \tag{10}$$

and define the source functional

$$l(v) := (\epsilon\kappa^2 I_b, v)_{L^2} + (\epsilon\kappa I_b, \mathbf{s}\cdot\boldsymbol{\nabla}_x v)_{L^2}. \tag{11}$$

Then the resulting linear variational problem reads: Find $\tilde{u} \in \mathcal{V}_0$ such that

$$a(\tilde{u}, v) = l(v) \quad \forall v \in \mathcal{V}_0. \tag{12}$$

For $d = 2$ we further require that there is a constant $0 < C < \infty$ such that

$$\|u\|_{L^2} \leq C\|\mathbf{s}\cdot\boldsymbol{\nabla}_x u\|_{L^2} \quad \forall u \in \mathcal{V}, \tag{13}$$

for $d = 3$ the Poincaré-Friedrichs inequality ensures the same relation. Then the following theorem holds (Widmer 2009, Thm. 2.2).

Theorem 2.1. *For every non-negative and bounded κ, the bilinear form $a(u,v)$ is continuous on $\mathcal{V}\times\mathcal{V}$ and coercive on $\mathcal{V}_0\times\mathcal{V}_0$ equipped with the norm $\|\cdot\|_S$. In particular, for every $I_b \in L^2(D)$, there exists a unique weak solution $\tilde{u} \in \mathcal{V}_0$ of the stabilized variational form* (12) *of the radiative transfer problem* (2)*.*

Although the proofs by Manteuffel et al. (2000) are restricted to piecewise constant absorption coefficients, the extension to non-constant coefficients is straightforward (see Widmer 2009).

As the bilinear form $a(\cdot,\cdot)$ is symmetric and positive definite on $\mathcal{V}_0$, the expression

$$\|u\|_A := \sqrt{a(u,u)} \tag{14}$$

defines a norm on $\mathcal{V}_0$, to which we will refer as "energy", or $A(D\times\mathcal{S}^{d_S})$ norm below.

3 Galerkin discretization

For the discretization, we follow Widmer et al. (2007). We are going to search for solutions to the variational problem (12) in the space

$$V_0 := H^{1,0}(D \times \mathcal{S}^{d_S}) \cap \mathcal{V}_0, \quad H^{1,0}(D \times \mathcal{S}^{d_S}) = H^1(D) \otimes L^2(\mathcal{S}^{d_S}). \tag{15}$$

According to Thm. 2.1 the variational problem (12) is well-posed on $\mathcal{V}_0$, therefore we also obtain well-posedness on the proper, closed subspace V_0 of $\mathcal{V}_0$. We furthermore assume that the weak solutions $\tilde{u} \in \mathcal{V}_0$ and $\bar{u} \in V_0$, of (12) with homogeneous Dirichlet data $g = 0$, coincide and denote this solution by u. This regularity assumption states that the weak solution $u \in \mathcal{V}$ of (2) with $g = 0$ belongs, in fact, to $H^1(D) \otimes L^2(\mathcal{S}^{d_S})$. Note that this assumption excludes line discontinuities of u in D which may arise due to transport along rays of discontinuous boundary data.

The variational problem (12) with homogeneous Dirichlet data is then discretized by restricting $u = \tilde{u}$ and v in the weak formulation (12) to a parameterized family of finite dimensional subspaces $\{V_0^{L,N}\}_{L,N}$ of V_0, where the superscript L will denote level of physical "refinement" and N level of angular "refinement" defined below. This yields

$$u_{L,N} \in V_0^{L,N} : \quad a(u_{L,N}, v) = l(v) \quad \forall v \in V_0^{L,N}. \tag{16}$$

As $a(\cdot,\cdot)$ is coercive and continuous on $\mathcal{V}_0 \times \mathcal{V}_0$, Eq. (16) has a unique solution which satisfies the Galerkin orthogonality

$$\forall v \in V_0^{L,N} : \qquad a(u - u_{L,N}, v) = 0. \tag{17}$$

The error $e_{L,N} = u - u_{L,N}$ is therefore quasioptimal in the $\| \cdot \|_S$-norm, i. e. for every subspace $V_0^{L,N}$ in the sequence, we obtain

$$\|u - u_{L,N}\|_S \leq C(\kappa, D) \inf_{v_{L,N} \in V_0^{L,N}} \|u - v_{L,N}\|_S. \tag{18}$$

Since the domain $D \times \mathcal{S}^{d_S}$ is a cartesian product domain, the subspace sequences $V_0^{L,N}$ will be built of tensor products of hierarchic finite dimensional subspaces of D and of $\mathcal{S}^{d_S}$, respectively. Due to the $\mathbf{s}$ dependence of the Dirichlet boundary $\Gamma_-(\mathbf{s}) \subset \partial D$, however, the subspaces $V_0^{L,N}$ will generally *not* be of tensor product type once the boundary condition (2b) is imposed. To deal with this problem and to retain a tensor-product-like structure for the case with boundary conditions we will split up the physical function space in Section 3.3 and tensorize subspaces so that only conforming product combinations are created.

Here we will start with the construction of the component spaces without boundary conditions. To this end, we equip the physical domain D with a triangular or rectangular ($d = 2$) or tetrahedral or cubic ($d = 3$) mesh $\mathcal{T}_D^0$. Nested mesh sequences $\mathcal{T}_D^l$, $l = 1, ..., L$, are then obtained by dyadic refinement of the coarse mesh $\mathcal{T}_D^0$.

We then specify the finite element space on D on the nested mesh sequences as

$$V_D^l := S^{p,1}(D, \mathcal{T}_D^l) \subset H^1(D). \tag{19}$$

It consists of piecewise polynomial functions of degree $p \geq 1$ on the mesh $\mathcal{T}_D^l$ which are continuous in D. For $l = 1, \ldots, L$, we obtain a sequence of hierarchic finite dimensional subspaces

$$V_D^0 \subset V_D^1 \subset \ldots \subset V_D^L \subset H^1(D),$$

with the dimension $M_D := \dim V_D^L$.

In the angular domain $\mathcal{S}^{d_\mathcal{S}}$, we use a spectral discretization, in contrast to wavelets which were employed by Widmer et al. (2007). Harmonic functions $S_{n,m}^{(d_\mathcal{S})} \in L^2(\mathcal{S}^{d_\mathcal{S}})$ up to order N as defined in Section 3.1.1 span the function space

$$V_\mathcal{S}^N := \mathbb{P}_N^{d_\mathcal{S}} = \text{span}\{S_{n,m}^{(d_\mathcal{S})} : n = 0, \ldots, N;\ m = 1, \ldots, m_{n,d_\mathcal{S}}\}. \tag{20}$$

As the harmonics have global support, we do not require an underlying mesh to be defined on $\mathcal{S}^{d_\mathcal{S}}$. The definition of the angular function space also gives rise to a sequence of hierarchic subspaces on the angular domain

$$V_\mathcal{S}^0 \subset V_\mathcal{S}^1 \subset \ldots \subset V_\mathcal{S}^N \subset L^2(\mathcal{S}^{d_\mathcal{S}}),$$

with the dimension $M_\mathcal{S} := \dim V_\mathcal{S}^N$.

Based on the function spaces V_D^L and $V_\mathcal{S}^N$ in the component domains D and $\mathcal{S}^{d_\mathcal{S}}$, we define the tensor product space $V_0^{L,N} \subset V_0$ by

$$V_0^{L,N} := (V_D^L \otimes V_\mathcal{S}^N) \cap \mathcal{V}_0 = (S^{p,1}(D, \mathcal{T}_D^L) \otimes \mathbb{P}_N^{d_\mathcal{S}}) \cap \mathcal{V}_0. \tag{21}$$

The Galerkin discretized problem then reads: find $u_{L,N}(\mathbf{x}, \mathbf{s}) \in V_0^{L,N}$ such that

$$a(u_{L,N}, v_{L,N}) = l(v_{L,N}) \qquad \forall v_{L,N} \in V_0^{L,N}. \tag{22}$$

Let $\{\alpha_i(\mathbf{x})\}_{i=1}^{M_D}$ be a basis of V_D^L and $\{\beta_j(\mathbf{s})\}_{j=1}^{M_\mathcal{S}}$ a basis of $V_\mathcal{S}^L$. Then the approximate intensity $u_{L,N} \in V^{L,N} := V_D^L \otimes V_\mathcal{S}^N$ can be expressed in the tensor product form

$$u_{L,N}(\mathbf{x}, \mathbf{s}) = \sum_{i=1}^{M_D} \sum_{j=1}^{M_\mathcal{S}} u_{ij} \alpha_i(\mathbf{x}) \beta_j(\mathbf{s}). \tag{23}$$

The discretized problem (22) then leads to a linear system of equations for the $M_D \cdot M_\mathcal{S}$ unknowns u_{ij}.

A natural choice of bases in the simplest case $p = 1$ (continuous, piecewise linear elements in D) are locally supported piecewise linear "hat functions" for V_D^L, that is $\alpha_i(x_j) = \delta_{ij}$, where $\{x_1, ..., x_{M_D}\}$ is the set of vertices of $\mathcal{T}_D^L$. The angular basis functions β_j are chosen to be harmonics $S_{n,m}^{(1)}$ on the circle $\mathcal{S}^1$ (trigonometric functions) or spherical harmonics $S_{n,m}^{(2)}$ on the sphere $\mathcal{S}^2$ as defined in Section 3.1.1. In the following, we are going to use the term harmonics to refer to both the harmonics on the circle and the spherical harmonics.

As the total number of degrees of freedom is $M_D \cdot M_\mathcal{S}$, where M_D and $M_\mathcal{S}$ are the number of basis functions in physical space and angular space, respectively, this approach turns out to be very expensive.

One way to reduce the total number of degrees of freedom is the use of *adapted bases* that offer a good representation of the solution with only a few degrees of freedom. However, adaptivity usually requires an iterative procedure to identify the most relevant degrees of freedom.

Here, we propose an a-priori-selection of degrees of freedom that are likely to be relevant for smooth solutions. Often only a few of the product basis functions $\alpha_i(\mathbf{x})\beta_j(\mathbf{s})$, $i = 1, \ldots, M_D$, $j = 1, \ldots, M_{\mathcal{S}}$, as in (23), really make a significant contribution to the representation of the final solution. Hence, a promising approach to obtaining efficient trial spaces is to select a few important *combined basis functions* of the form $\alpha_i(\mathbf{x})\beta_j(\mathbf{s})$ and let them span $V^{L,N}$. The *component basis functions* α_i and β_j can be chosen from large, even infinite sets, which will not translate into prohibitively large discrete problems. This idea underlies the present approach to the Galerkin discretization of the radiative transfer problem which is based on *sparse tensor products* of the *hierarchic* component finite element spaces V_D^L and $V_{\mathcal{S}}^N$.

3.1 Angular basis functions

3.1.1 Definition of harmonics

In the case $d_{\mathcal{S}} = 1$, we choose the real Fourier basis of sine and cosine functions to expand functions on the circle. These basis functions $S_{n,m}^{(1)} : [0, 2\pi] \to \mathbb{R}$ are defined as

$$S_{n,m}^{(1)}(\varphi) := \begin{cases} \frac{1}{\sqrt{2\pi}} & \text{if } n = 0, \\ \frac{1}{\sqrt{\pi}} \sin(n\varphi) & \text{if } n > 0 \text{ and } m = 1, \\ \frac{1}{\sqrt{\pi}} \cos(n\varphi) & \text{if } n > 0 \text{ and } m = 2, \end{cases} \tag{24}$$

with $n \in \mathbb{N}_0$ and $m \in \{1, 2\}$ for $n > 0$. This simplifies the combined treatment of the one- and two-dimensional case later on.

For basis functions for $d_{\mathcal{S}} = 2$ in the angular domain $\mathcal{S}^2$, we select real-valued spherical harmonics as e. g. Blanco et al. (1997) to avoid complex arithmetics. These real-valued spherical harmonics $S_{n,m}^{(2)} : [0, \pi] \times [0, 2\pi] \to \mathbb{R}$ are obtained from a linear combination of the complex-valued spherical harmonics $Y_{n,\tilde{m}}$ of the same order n:

$$S_{n,m}^{(2)} := \begin{cases} \frac{(-1)^{\tilde{m}}}{\sqrt{2}} (Y_{n,\tilde{m}} + (-1)^{\tilde{m}} Y_{n,-\tilde{m}}) & \text{if } \tilde{m} > 0, \\ Y_{n,0} & \text{if } \tilde{m} = 0, \\ \frac{(-1)^{\tilde{m}}}{\sqrt{2}i} (Y_{n,-\tilde{m}} - (-1)^{\tilde{m}} Y_{n,\tilde{m}}) & \text{if } \tilde{m} < 0, \end{cases} \tag{25}$$

in which $-n \le \tilde{m} \le n$ and $\tilde{m} = m - n - 1$ so that $m = 1, \ldots, 2n + 1$.

The index m for basis functions of the same order n has the maximum value $m_{n,d_{\mathcal{S}}}$, which is

$$\begin{array}{ll} m_{n,1} = 2 & \text{for } d_{\mathcal{S}} = 1, \\ m_{n,2} = 2n + 1 & \text{for } d_{\mathcal{S}} = 2. \end{array} \tag{26}$$

3.1.2 Properties of harmonics

Any function $f \in L^2(\mathcal{S}^{d_\mathcal{S}})$ can be represented in the basis of harmonics as

$$f(\mathbf{s}) = \sum_{n=0}^{\infty} \sum_{m=1}^{m_{n,d_\mathcal{S}}} a_{n,m} S_{n,m}^{(d_\mathcal{S})}(\mathbf{s}), \tag{27}$$

with Fourier coefficients $a_{n,m}$ determined from

$$a_{n,m} = (f, S_{n,m}^{(d_\mathcal{S})})_{L^2(\mathcal{S}^{d_\mathcal{S}})}. \tag{28}$$

The expansion of a function in spherical basis functions has a number of useful relations to its derivatives on the sphere. In spherical coordinates $(\varrho, \vartheta_1, \ldots, \vartheta_{d_\mathcal{S}})$, the Laplacian is given by

$$\Delta = \frac{\partial^2}{\partial \varrho^2} + \frac{d_\mathcal{S}}{\varrho} \frac{\partial}{\partial \varrho} - \frac{1}{\varrho^2} \delta, \tag{29}$$

where the *Beltrami operator* δ contains the angular part of the Laplacian of the form

$$\delta = -\sum_{j=1}^{d_\mathcal{S}} \frac{1}{q_j \sin^{d_\mathcal{S}-j} \vartheta_j} \frac{\partial}{\partial \vartheta_j} \left(\sin^{d_\mathcal{S}-j} \vartheta_j \frac{\partial}{\partial \vartheta_j} \right), \tag{30}$$

$$q_1 = 1, \quad q_j = (\sin \vartheta_1 \ \sin \vartheta_2 \ \ldots \ \sin \vartheta_{j-1})^2, \ j > 1. \tag{31}$$

The expansion coefficients $b_{n,m}$ in terms of harmonics of the t-th power of the Beltrami operator can now be expressed by the expansion coefficients $a_{n,m}$ of the original function $f \in D(\delta^t)$, the domain of δ^t, by (see Mikhlin and Prössdorf 1986, Ch. 8, §4, Eq. 8)

$$b_{n,m} = n^t (n + d_\mathcal{S} - 1)^t a_{n,m}. \tag{32}$$

For $t \in \mathbb{N}_0$, the t-th power of the Beltrami therefore has the spherical expansion

$$\delta^t f(\mathbf{s}) = \sum_{n=1}^{\infty} \sum_{m=1}^{m_{n,d_\mathcal{S}}} n^t (n + d_\mathcal{S} - 1)^t a_{n,m} S_{n,m}^{(d_\mathcal{S})}(\mathbf{s}), \tag{33}$$

and for its L^2-norm, it holds the Parseval equation

$$\|\delta^t f\|^2_{L^2(\mathcal{S}^{d_\mathcal{S}})} = \sum_{n=1}^{\infty} \sum_{m=1}^{m_{n,d_\mathcal{S}}} n^{2t} (n + d_\mathcal{S} - 1)^{2t} |a_{n,m}|^2. \tag{34}$$

From this equation, we see that the domain of δ^t, $D(\delta^t)$, consists of those functions for which

$$\sum_{n=1}^{\infty} \sum_{m=1}^{m_{n,d_\mathcal{S}}} n^{4t} |a_{n,m}|^2 < \infty \tag{35}$$

is satisfied. We can also rewrite (34) in the form

$$\|\delta^{t/2} f\|^2_{L^2(\mathcal{S}^{d_\mathcal{S}})} = \sum_{n=1}^{\infty} \sum_{m=1}^{m_{n,d_\mathcal{S}}} n^t (n + d_\mathcal{S} - 1)^t |a_{n,m}|^2. \tag{36}$$

For odd t, $\delta^{t/2}$ is understood in the sense of interpolation of linear operators (see e. g. Triebel 1995, Sec. 1.15.1, for the definition). Then we finally arrive at the following theorem:

Theorem 3.1. *For a function $f \in H^t(\mathcal{S}^{d_\mathcal{S}}) \cap D(\delta^{t/2} f) \cap \bar{L}^2(\mathcal{S}^{d_\mathcal{S}})$, where $\bar{L}^2(\mathcal{S}^{d_\mathcal{S}})$ is the subspace of $L^2(\mathcal{S}^{d_\mathcal{S}})$ orthogonal to 1, $t > 0$, we obtain the estimate for its H^t-norm*

$$\|f\|_{H^t(\mathcal{S}^{d_\mathcal{S}})} \simeq \|\delta^{t/2} f\|_{L^2(\mathcal{S}^{d_\mathcal{S}})}, \tag{37}$$

where the symbol $\simeq$ is the abbreviation for a two-sided estimate with positive constants independent from f.

The proof is given e. g. by Mikhlin and Prössdorf (1986, Ch. 8, §4, Thm. 4.1).

3.1.3 Definition of Legendre polynomials on angular regions

In the $(d, d_\mathcal{S}) = (2, 1)$ case, we can choose Legendre polynomials as basis functions on the angular regions $S_q = [\varphi_1, \varphi_2] \subset \mathcal{S}^1$.

Let $L_n(x)$ be the normalized Legendre polynomials which are L^2-orthonormal on $[-1, 1]$. We map the polynomials to S_q via an affine transformation $X_q(\varphi)$ to obtain basis functions $S_{n,m}^{(1,q)}$ on an angular region:

$$S_{n,m}^{(1,q)}(\varphi) := \begin{cases} L_0(X_q(\varphi)) & \text{if } n = 0 \\ L_{2n+m-2}(X_q(\varphi)) & \text{if } n > 0 \end{cases}, \quad n = 0, \ldots, N; m = 1, 2. \tag{38}$$

They conform to the notation of the harmonics on the circle with an additional index q for the angular region.

3.2 Sparse tensor product space without boundary conditions

The radiative transfer equation (2a) loses tensor product structure when inflow boundary conditions (2b) are added. Additionally, Dirichlet boundary conditions on the sphere can only be satisfied approximately if we choose harmonics on the full sphere as basis functions. The degrees of freedom associated with our product basis functions involving harmonics are not pointwise degrees of freedom on the sphere, therefore simply setting some of them to zero does not satisfy the zero inflow boundary conditions.

In Marshak's formulation of the boundary conditions (see e. g. Modest 2003), additional conditions for the degrees of freedom are derived from integral equations over the inflow hemispheres at points on the boundary. Another option would be the inclusion of an additional term in the least squares minimization functional (4) which penalizes the deviation of the solution from the boundary conditions (Manteuffel et al. 2000).

However, these approaches only lead to weakly satisfied boundary conditions. In a later section, we present a method to obtain satisfaction of the boundary conditions in a strong sense by employing basis functions that are V_0-conforming. For the derivation of approximation properties of the function spaces in this section, however, we are going to disregard the boundary conditions for ease of exposition.

3.2.1 Definition

To find those product basis functions which contribute significantly to the solution, we proceed in the same manner as Widmer et al. (2007) in principle.

For finite element spaces with an underlying grid, the framework of sparse grids (Bungartz and Griebel 2004) provides an approach to reduce the number of basis functions without compromising accuracy under certain smoothness assumptions. On nested, hierarchical sets of grids refined up to a level l, sets of basis functions which preserve this hierarchical property are defined so that each set of functions can be associated with the level of resolution. Basis functions of lower level usually contribute significantly to the approximation of smooth functions, for basis functions of higher levels, the contribution generally reduces with increasing level.

In the construction of sparse tensor product spaces in $H^{1,0}(D \times \mathcal{S}^{d_\mathcal{S}}) \simeq H^1(D) \otimes L^2(\mathcal{S}^{d_\mathcal{S}})$, we exploit the hierarchic multilevel structure of the sets of basis functions $\{\alpha_i\}_i$ and $\{\beta_j\}_j$. On the physical domain D, this structure arises from the nested meshes $\mathcal{T}_D^l$, with $l = 0, 1, 2, \ldots$, the level index. Recall from (19) the definition of the corresponding nested sequence of finite element spaces

$$V_D^l := S^{p,1}(D, \mathcal{T}_D^l) \subset H^1(D).$$

In this, $S^{p,1}(D, \mathcal{T}_D^l)$ is the set of continuous, piecewise polynomial functions of degree $p \geq 1$ on $\mathcal{T}_D^l$. Furthermore, we can define "detail" or "increment" spaces W_D^l such that

$$V_D^l = W_D^l \oplus V_D^{l-1}, \tag{39}$$

where $\oplus$ denotes the direct sum.

In contrast to Widmer et al. (2007), we use harmonics $S_{n,m}^{(d_\mathcal{S})}$ as basis functions in the angular domain $\mathcal{S}^{d_\mathcal{S}}$, for which the hierarchical structure is inherent. The index n of their order corresponds to the level of resolution l. The nested sequence of angular function spaces was defined in (20) by

$$V_\mathcal{S}^l := \mathbb{P}_l^{d_\mathcal{S}} = \operatorname{span}\{S_{n,m}^{(d_\mathcal{S})} : n = 0, \ldots, l;\ m = 1, \ldots, m_{n,d_\mathcal{S}}\}. \tag{40}$$

A detail space on $\mathcal{S}^{d_\mathcal{S}}$ comprises the harmonics of level l:

$$W_\mathcal{S}^l = \operatorname{span}\{S_{n,m}^{(d_\mathcal{S})} : n = l;\ m = 1, \ldots, m_{n,d_\mathcal{S}}\} \quad \Rightarrow \quad V_\mathcal{S}^l = W_\mathcal{S}^l \oplus V_\mathcal{S}^{l-1}, \tag{41}$$

due to L^2-orthogonality of the harmonics. The maximum inner index $m_{n,d_\mathcal{S}}$ may depend on the current n and dimension $d_\mathcal{S}$ and was defined in Eq. (26).

Both on the physical and angular domain, we can therefore compose the spaces V_D^l and $V_\mathcal{S}^l$ of sequences of L^2-orthogonal detail subspaces:

$$V_D^l = \bigoplus_{i=0}^{l} W_D^i, \quad V_\mathcal{S}^l = \bigoplus_{i=0}^{l} W_\mathcal{S}^i, \tag{42}$$

where we set $W_D^0 := V_D^0$ and $W_\mathcal{S}^0 := V_\mathcal{S}^0$, respectively. With these definitions, the full tensor product space $V^{L,N} \subset H^1(D) \otimes L^2(\mathcal{S}^{d_\mathcal{S}})$ at level L and order N is given by

$$V^{L,N} = V_D^L \otimes V_\mathcal{S}^N = \bigoplus_{\substack{0 \leq l_D \leq L \\ 0 \leq l_\mathcal{S} \leq N}} W_D^{l_D} \otimes W_\mathcal{S}^{l_\mathcal{S}}. \tag{43}$$

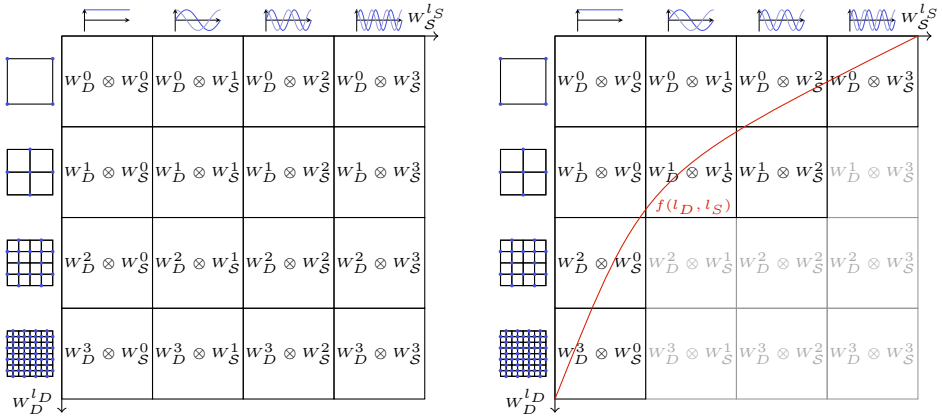

Figure 1: Full (left) and sparse (right) tensor product space structure for $V_D^{L=3} = S^{(1,1)}([0,1]^2, \mathcal{T}_D^3)$ and $V_{\mathcal{S}}^{N=3} = \mathbb{P}_3^1$.

In the following we are going to consider the sparse tensor product space $\hat{V}^{L,N} \subset V^{L,N}$ defined by

$$\hat{V}^{L,N} := \bigoplus_{0 \le f(l_D, l_S) \le L} W_D^{l_D} \otimes W_{\mathcal{S}}^{l_S}, \tag{44}$$

where the cutoff function $f : [0, L] \times [0, N] \to \mathbb{R}$ determines which detail tensor product spaces are included in the sparse tensor product space. It is further specified for our method later. Analogously to $V_0^{L,N} := V^{L,N} \cap \mathcal{V}_0$ from Eq. (21), we set

$$\hat{V}_0^{L,N} \subset \hat{V}^{L,N} \cap \mathcal{V}_0. \tag{45}$$

By Eq. (23), the dimension of the full tensor product space equals

$$\dim(V_0^{L,N}) = M_{\mathcal{S}} M_D, \tag{46}$$

and the dimension of the sparse tensor product space depends on the selected cutoff function f.

3.2.2 Approximation properties

Preliminaries. As the sparse tensor product space contains fewer elements than the full tensor product space, accuracy may be lost. In this section, we are going to compare the rate of convergence of the sparse Galerkin approximations to the solution u to the rate obtained with a full Galerkin approximation. We will find that, at least for smooth solutions, both spaces achieve the same asymptotic convergence rate.

For this purpose we define the L^2-projection operators $P_D^l : L^2(D) \to V_D^l$ and $P_{\mathcal{S}}^l : L^2(\mathcal{S}^{d_S}) \to V_{\mathcal{S}}^l$ with the convention that $P_D^{-1} = P_{\mathcal{S}}^{-1} = 0$. The projector $P_{L,N}$

onto the full tensor product space of level L is given by

$$u_{L,N}(\mathbf{x},\mathbf{s}) = P_{L,N}u(\mathbf{x},\mathbf{s}) := \sum_{\substack{0\le l_D\le L\\ 0\le l_S\le N}} \left(P_D^{l_D} - P_D^{l_D-1}\right)\otimes\left(P_{\mathcal{S}}^{l_S} - P_{\mathcal{S}}^{l_S-1}\right) u(\mathbf{x},\mathbf{s}). \quad (47)$$

The projector $\widehat{P}_{L,N}$ onto the sparse tensor product space of level L accordingly reads

$$\widehat{u}_L(\mathbf{x},\mathbf{s}) := \widehat{P}_{L,N}u(\mathbf{x},\mathbf{s}) := \sum_{0\le f(l_D,l_S)\le L} \left(P_D^{l_D} - P_D^{l_D-1}\right)\otimes\left(P_{\mathcal{S}}^{l_S} - P_{\mathcal{S}}^{l_S-1}\right) u(\mathbf{x},\mathbf{s}). \quad (48)$$

The function $f(l_D, l_S)$ determines the cutoff of the original full tensor product space to the sparse tensor product space. If the condition $0 \le f(l_D, l_S) \le L$ is satisfied for a pair (l_D, l_S), we include the detail tensor product space $W_D^{l_D} \otimes W_{\mathcal{S}}^{l_S}$ in the sparse tensor product space $\hat{V}_0^{L,N}$.

In order to describe the approximation properties of the sparse tensor product space $\widehat{V}_L$, we follow Griebel et al. (1999) and von Petersdorff and Schwab (2004) and introduce anisotropic Sobolev spaces with fractional derivatives. We start by defining the anisotropic Sobolev spaces

$$H^{s,t}(D\times\mathcal{S}^{d_{\mathcal{S}}}) := H^s(D)\otimes H^t(\mathcal{S}^{d_{\mathcal{S}}}) \quad (49)$$

which are, for integer values of s and of t, given by

$$\left\{u\in L^2(D\times\mathcal{S}^{d_{\mathcal{S}}}) \,|\, D_{\mathbf{x}}^{\alpha}D_{\mathbf{s}}^{\beta}u \in L^2(D\times\mathcal{S}^{d_{\mathcal{S}}}),\ 0\le|\alpha|\le s,\ 0\le|\beta|\le t\right\}, \quad (50)$$

where for $\alpha\in\mathbb{N}_0^d$, $D_{\mathbf{x}}^{\alpha}$ denotes the α-th weak derivative with respect to $\mathbf{x}\in D$; we denote its order by $|\alpha| = \alpha_1 + \ldots + \alpha_d$. Analogously, for $\beta\in\mathbb{N}_0^{d_{\mathcal{S}}}$, $D_{\mathbf{s}}^{\beta}$ denotes the weak derivative with respect to $\mathbf{s}\in\mathcal{S}^{d_{\mathcal{S}}}$ and we denote its order $|\beta| = \beta_1 + \ldots + \beta_{d_{\mathcal{S}}}$.

We equip the anisotropic space with the norm

$$\|u\|_{H^{s,t}}^2 := \sum_{\substack{0\le|\alpha|\le s\\ 0\le|\beta|\le t}} \|D_{\mathbf{x}}^{\alpha}D_{\mathbf{s}}^{\beta}u\|_{L^2(D\times\mathcal{S}^{d_{\mathcal{S}}})}^2. \quad (51)$$

For arbitrary $s,t\ge 0$, we define $H^{s,t}(D\times\mathcal{S}^{d_{\mathcal{S}}})$ by interpolation.

Error estimates on physical and angular domain. For functions $v(\mathbf{x})\in H^{s+1}(D)$, $s\in[0,\ p]$, the following approximation properties hold for $l\in\mathbb{N}_0$ (see e. g. Nguyen 2005, Lemma 2.3.1):

$$\|v - P_D^l v\|_{H^1(D)} \lesssim 2^{-ls}\|v\|_{H^{s+1}(D)},\ s\in[0,\ p]. \quad (52)$$

Here and in the following, we use the notations $a\lesssim b$ ($a\simeq b$) if there exists a constant $0<C<\infty$ with $a\le Cb$ ($a\le Cb$ and $a\ge C^{-1}b$). The constants in these estimates may depend on the angles in the mesh $\mathcal{T}_D^0$ and on the dimensions d and $d_{\mathcal{S}}$.

Next, we prove an error estimate on the angular domain.

Lemma 3.2. *For $w(\mathbf{s}) \in H^t(\mathcal{S}^{d_\mathcal{S}})$, $t \in \mathbb{N}_0$, the approximation error of the expansion of w in harmonics up to order N is given by*

$$\left\|w - P_\mathcal{S}^N w\right\|_{L^2(\mathcal{S}^{d_\mathcal{S}})} \lesssim N^{-t} \left\|w\right\|_{H^t(\mathcal{S}^{d_\mathcal{S}})}, \tag{53}$$

where $t \in \mathbb{N}_0$.

Proof. We use the harmonic series representation from (27) for w and Parseval's theorem to express the square of the approximation error as an infinite series:

$$\begin{aligned}\left\|w - P_\mathcal{S}^N w\right\|^2_{L^2(\mathcal{S}^{d_\mathcal{S}})} &= \sum_{n=N+1}^{\infty} \sum_{m=1}^{m_{n,d_\mathcal{S}}} |a_{n,m}|^2 \cdot \underbrace{n^{-t}(n+d_\mathcal{S}-1)^{-t} n^t (n+d_\mathcal{S}-1)^t}_{=1} \\ &\leq (N+1)^{-t}(N+d_\mathcal{S})^{-t} \sum_{n=N+1}^{\infty} \sum_{m=1}^{m_{n,d_\mathcal{S}}} |a_{n,m}|^2 n^t (n+d_\mathcal{S}-1)^t\end{aligned}$$

by factoring out the maximum of the first term. With (36) and Thm. 3.1

$$\begin{aligned}\left\|w - P_\mathcal{S}^N w\right\|^2_{L^2(\mathcal{S}^{d_\mathcal{S}})} &\leq ((N+1)(N+d_\mathcal{S}))^{-t} \sum_{n=1}^{\infty} \sum_{m=1}^{m_{n,d_\mathcal{S}}} |a_{n,m}|^2 n^t (n+d_\mathcal{S}-1)^t \\ &= ((N+1)(N+d_\mathcal{S}))^{-t} \|\delta^{t/2} w\|^2_{L^2(\mathcal{S}^{d_\mathcal{S}})} \\ &\simeq ((N+1)(N+d_\mathcal{S}))^{-t} \|w\|^2_{H^t(\mathcal{S}^{d_\mathcal{S}})} \\ &\leq N^{-2t} \|w\|^2_{H^t(\mathcal{S}^{d_\mathcal{S}})}.\end{aligned}$$

Taking the square root of both sides yields the statement of the lemma. □

Error estimate for full tensor product space. With the previous lemma and the error estimate (52) in the physical domain, we can derive estimates for the approximation on the tensor product spaces. First we consider the full tensor product case.

Theorem 3.3. *The Galerkin approximation $u_{L,N}$ on the full tensor product space $V_0^{L,N}$ of a function $u \in H^{s+1,t}(D \times \mathcal{S}^{d_\mathcal{S}})$, $s \in [0,p]$, $t \in \mathbb{N}_0$, satisfies the asymptotic error estimate*

$$\|u - P_{L,N} u\|_{H^{1,0}(D \times \mathcal{S}^{d_\mathcal{S}})} \lesssim \max\{M_\mathcal{S}^{-t/d_\mathcal{S}}, M_D^{-s/d}\} \|u\|_{(H^{1,t} \cap H^{1+s,0})(D \times \mathcal{S}^{d_\mathcal{S}})}, \tag{54}$$

depending on the number of physical degrees of freedom M_D and angular degrees of freedom $M_\mathcal{S}$ related to L, N by $M_D \simeq 2^{dL}$ and $M_\mathcal{S} \simeq N^{d_\mathcal{S}}$.

Proof. The asymptotic density of the discrete subspace sequences in $H^1(D) \otimes L^2(\mathcal{S}^{d_\mathcal{S}})$ permits us to write any function $u \in H^1(D) \otimes L^2(\mathcal{S}^{d_\mathcal{S}})$ uniquely as

$$u(\mathbf{x}, \mathbf{s}) = \sum_{l_D, l_\mathcal{S}=0}^{\infty} u_{l_D, l_\mathcal{S}}(\mathbf{x}, \mathbf{s}), \quad u_{l_D, l_\mathcal{S}} \in W_D^{l_D} \otimes W_\mathcal{S}^{l_\mathcal{S}}.$$

We can therefore estimate the $H^{1,0}$ norm of the approximation error by (the domain $D \times \mathcal{S}^{d_S}$ has been omitted in the following)

$$\begin{aligned}\|u - P_{L,N}u\|_{H^{1,0}} &= \left\| \sum_{l_D=0}^{L} \sum_{l_S=N+1}^{\infty} u_{l_D,l_S} + \sum_{l_D=L+1}^{\infty} \sum_{l_S=0}^{\infty} u_{l_D,l_S} \right\|_{H^{1,0}} \\ &\leq \left\| P_D^L \otimes (\mathrm{Id} - P_S^N)u \right\|_{H^{1,0}} + \left\| (\mathrm{Id} - P_D^L) \otimes \mathrm{Id}\, u \right\|_{H^{1,0}} \\ &\leq \left\| \mathrm{Id} \otimes (\mathrm{Id} - P_S^N)u \right\|_{H^{1,0}} + \left\| (\mathrm{Id} - P_D^L) \otimes \mathrm{Id}\, u \right\|_{H^{1,0}}.\end{aligned}$$

The first term can be estimated by Lemma 3.2, the second by (52), to yield

$$\begin{aligned}\|u - P_{L,N}u\|_{H^{1,0}} &\lesssim N^{-t} \|u\|_{H^{1,t}} + 2^{-Ls} \|u\|_{H^{1+s,0}} \\ &\lesssim \max\{N^{-t}, 2^{-Ls}\} \|u\|_{(H^{1,t} \cap H^{1+s,0})}.\end{aligned}$$

Expressed in terms of numbers of degrees of freedom, we can state the estimate

$$\|u - P_{L,N}u\|_{H^{1,0}} \lesssim \max\{N^{-t}, 2^{-Ls}\} \|u\|_{(H^{1,t} \cap H^{1+s,0})} \tag{55}$$

$$\simeq \max\{M_{\mathcal{S}}^{-t/d_{\mathcal{S}}}, M_D^{-s/d}\} \|u\|_{(H^{1,t} \cap H^{1+s,0})}, \tag{56}$$

using the relations $M_D \simeq 2^{dL}$ and $M_{\mathcal{S}} \simeq N^{d_{\mathcal{S}}}$. □

An increase of the number of degrees of freedom M_D and $M_{\mathcal{S}}$ is most effective in terms of error reduction if the error contributions from the discretizations in physical and angular space are of the same order of magnitude. We would like to set

$$N^{-t} = 2^{-Ls} \quad \Rightarrow \quad N = 2^{Ls/t}, \tag{57}$$

but as s and t are often not known in applications we initially set $N = 2^L$. This defines the relation between N and L for the full tensor product case. With this choice of N, the error estimate finally becomes

$$\|u - P_{L,N}u\|_{H^{1,0}} \lesssim h^{\min\{t,s\}} \|u\|_{(H^{1,t} \cap H^{1+s,0})}, \tag{58}$$

where $h < 1$, the mesh size in the physical domain D, is related to L by $h \simeq 2^{-L}$. Here, the smaller smoothness determines the convergence rate.

Optimally with $N = 2^{Ls/t}$, the order N of the harmonics must be increased reciprocally proportionally to the s/t-th power of the meshwidth to keep up with a reduction of the error on D when the mesh is refined. As s is limited by p, the increase in N can be all the slower the larger the angular smoothness t of the solution is.

Error estimates for sparse tensor product space. In the sparse tensor product case, we only include selected detail spaces into the search space. The choice of detail spaces is determined by the cutoff function $f(l_D, l_S)$, on which the final error estimates for the approximation

$$\|u - \widehat{P}_{L,N}u\|_{H^{1,0}} = \left\| \sum_{l_D=0}^{\infty} \sum_{l_S=\max\{0,\, l_{S,\max}+1\}}^{\infty} u_{l_D,l_S}(\mathbf{x}, \mathbf{s}) \right\|_{H^{1,0}} \tag{59}$$

depend. With $l_{S,\max}$ we denote the maximum feasible index value of l_S obtained by solving $f(l_D, l_S) = L$ w. r. t. l_S. The main result of this section is then summarized in

Theorem 3.4. *Let the cutoff function for the sparse tensor product space $\hat{V}_0^{L,N}$ be*

$$f(l_D, l_S) = l_D + \frac{L\lfloor \log_2(l_S+1)\rfloor}{\lfloor \log_2(N+1)\rfloor}, \tag{60}$$

then the Galerkin approximation $\widehat{u}_{L,N}$ on $\hat{V}_0^{L,N}$ of $u \in H^{s+1,t}(D \times \mathcal{S}^{d_\mathcal{S}})$, $s \in [0,p]$, $t \in \mathbb{N}_0$, satisfies the asymptotic error estimate

$$\|u - \widehat{P}_{L,N} u\|_{H^{1,0}(D\times\mathcal{S}^{d_\mathcal{S}})} \lesssim \log_2\left(M_D^{1/d}\right) \max\{M_D^{-s/d}, M_\mathcal{S}^{-t/d_\mathcal{S}}\} \|u\|_{H^{1+s,t}(D\times\mathcal{S}^{d_\mathcal{S}})}, \tag{61}$$

with the number of physical degrees of freedom M_D and angular degrees of freedom $M_\mathcal{S}$, again related to L, N by $M_D \simeq 2^{dL}$ and $M_\mathcal{S} \simeq N^{d_\mathcal{S}}$.

Proof. In order to develop our derivations along the lines of the wavelet case discussed by Widmer et al. (2007), we introduce a new index λ for the enumeration of the detail spaces in the angular domain:

$$\lambda := \lfloor \log_2(l_S+1)\rfloor \tag{62}$$

with $\Lambda := \lfloor \log_2(N+1)\rfloor$ the maximum value of the index and $\lfloor x\rfloor$ denoting rounding to the next integer less than or equal to x. As $l_S = 0, \ldots, N$, we get $\lambda = 0, \ldots, \Lambda$. Conversely, we are going to use $l_S = 2^{\lambda+1} - 2$ and $N = 2^{\Lambda+1} - 2$, respectively, so that for a certain value of λ, we set l_S to the largest possible value mapped to this λ. We also introduce the corresponding detail spaces W_S^λ defined by

$$W_S^\lambda := \bigoplus_{l_S = 2^{\lambda-1}}^{2^{\lambda+1}-2} W_S^{l_S}. \tag{63}$$

A detail space W_S^λ therefore essentially combines all the detail spaces $W_S^{l_S}$ for which $\lambda \le \log_2(l_S+1) < \lambda + 1$. On the product space indexed by l_D and λ, we define our sparse tensor product space with a linear cutoff between l_D and λ:

$$\hat{V}^{L,\Lambda} := \bigoplus_{0 \le l_D + \frac{L}{\Lambda}\lambda \le L} W_D^{l_D} \otimes W_S^\lambda. \tag{64}$$

With this tensorization, we have

$$\lambda \le \Lambda(1 - \frac{l_D}{L}) =: \lambda_{\max}. \tag{65}$$

As we have switched indexation on the angular domain from l_S to λ, we also have to express the error estimate on the angular domain given in Lemma 3.2 by λ. For this, we use the projector $P_S^\Lambda : L^2(\mathcal{S}^{d_\mathcal{S}}) \to V_S^\Lambda$, where $V_S^\Lambda = \bigoplus_{\lambda=0}^\Lambda W_S^\lambda$. Changing the

indexation doesn't affect the error estimate as long as we replace the quantities in N appropriately by their Λ representation:

$$\left\|w - P_{\mathcal{S}}^{N} w\right\|_{L^2(\mathcal{S}^{d_{\mathcal{S}}})} \lesssim N^{-t} \left\|w\right\|_{H^t(\mathcal{S}^{d_{\mathcal{S}}})}$$

becomes, after reformulations,

$$\left\|w - P_{S}^{\Lambda} w\right\|_{L^2(\mathcal{S}^{d_{\mathcal{S}}})} \lesssim (2^{\Lambda} - 1)^{-t} \left\|w\right\|_{H^t(\mathcal{S}^{d_{\mathcal{S}}})}.$$

As we are interested in large Λ, we get with $\Lambda \geq 1$

$$\left\|w - P_{S}^{\Lambda} w\right\|_{L^2(\mathcal{S}^{d_{\mathcal{S}}})} \lesssim 2^{-\Lambda t} \left\|w\right\|_{H^t(\mathcal{S}^{d_{\mathcal{S}}})}. \tag{66}$$

This error estimate resembles the error estimate for wavelets (Widmer et al. 2007):

$$\left\|w - P_{S}^{l} w\right\|_{L^2(\mathcal{S}^{d_{\mathcal{S}}})} \lesssim 2^{-lt} \left\|w\right\|_{H^t(\mathcal{S}^{d_{\mathcal{S}}})}, \quad t \in [0, q+1], \tag{67}$$

where q is the polynomial degree of the wavelets on the angular domain. Note, however, that our estimate (66) is valid for all $t > 0$. In theory, if the solution is sufficiently smooth, spectral convergence is not limited by a maximum smoothness value as given by q for wavelets.

The remaining part of the estimate is analogous to the one by Widmer et al. (2007), only instead of summing over l_S in (59), we now sum over λ:

$$\begin{aligned}\left\|u - \widehat{P}_{L,N} u\right\|_{H^{1,0}} &= \left\| \sum_{l_D=0}^{\infty} \sum_{\lambda=\max\{0,\, \lambda_{\max}+1\}}^{\infty} u_{l_D,\lambda}(\mathbf{x}, \mathbf{s}) \right\|_{H^{1,0}} \\ &\lesssim (L+2) 2^{-\min\{Ls, \Lambda t\}} \left\|u\right\|_{H^{1+s,t}}.\end{aligned}$$

In the product space indexed by l_D and l_S, the estimate transforms to

$$\left\|u - \widehat{P}_{L,N} u\right\|_{H^{1,0}} \leq (L+2) \max\{2^{-Ls}, N^{-t}\} \left\|u\right\|_{H^{1+s,t}}. \tag{68}$$

Expressed with the physical degrees of freedom $M_D \simeq 2^{dL}$ and the angular degrees of freedom $M_{\mathcal{S}} \simeq N^{d_{\mathcal{S}}}$, the estimate becomes

$$\left\|u - \widehat{P}_{L,N} u\right\|_{H^{1,0}} \lesssim \log_2\left(M_D^{1/d}\right) \max\{M_D^{-s/d}, M_{\mathcal{S}}^{-t/d_{\mathcal{S}}}\} \left\|u\right\|_{H^{1+s,t}}, \tag{69}$$

which we set out to prove. □

By equilibration of the terms in the estimate (68), we obtain $N = 2^{Ls/t}$, the same relation as in the full tensor case (57). Up to a logarithmic term, we retain the convergence rate (56) of the full tensor case while the number of employed degrees of freedom is significantly lower than $M_D \cdot M_{\mathcal{S}}$ of the full tensor case.

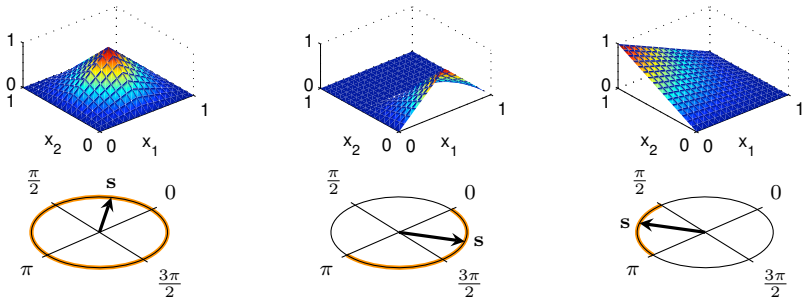

Figure 2: To obtain conforming product basis functions, the depicted physical basis functions over $D = [0,1]^2$ may only be tensorized with angular functions which are non-zero only on the associated outflow regions on $\mathcal{S}^1$ (marked).

3.3 Sparse tensor product space with boundary conditions

As it is not possible to exactly represent a function on the angular domain $\mathcal{S}^{d_S}$ that is zero on a d_S-dimensional region of the sphere by a truncated series of harmonics, we construct additional basis functions on the sphere which strictly satisfy the boundary conditions (2b).

For the $(d, d_S) = (2, 1)$ case, these basis functions could be e. g. trigonometric functions compressed to subintervals of $\mathcal{S}^1$, the circle. The harmonics are then effectively localized, which enables us to satisfy zero inflow boundary conditions in a strong sense if we tensorize matching compressed harmonics and basis functions $\alpha(\mathbf{x})$ on the boundary of the physical domain. Another possible choice are Legendre polynomials on subintervals of $\mathcal{S}^1$ as our solution is not periodic across the boundaries of the subintervals. They also offer a resolution index n, the order of the polynomial.

To obtain a V_0-conforming system, our goal in the construction of these additional basis functions therefore is that the boundary conditions will be satisfied naturally by our product basis functions. Product basis functions not conforming to the zero inflow condition will not be considered in the search space.

3.3.1 Definition

Assume that the physical domain D is a polyhedral domain with non-zero volume $\mathrm{Vol}(D) > 0$. This means that the border of D, ∂D, consists of a number K of planar faces F_k:

$$\partial D = \bigcup_{k=1}^{K} F_k. \tag{70}$$

We denote the interior of a face F_k by $\Gamma_k := F_k \setminus \partial F_k$ so that Γ_k is open. As all points $\mathbf{x}$ on a face Γ_k share the same outward unit normal $\mathbf{n}_k$, their outflow directions lie in

the same open hemisphere Σ_k:

$$\Sigma_k := \{\mathbf{s} \in \mathcal{S}^{d_\mathcal{S}} : \mathbf{s} \cdot \mathbf{n}_k > 0\}. \tag{71}$$

Remark 1. We are going to ignore the limit case $\mathbf{s} \cdot \mathbf{n}(\mathbf{x}) = 0$ and the boundaries of the faces F_k since they constitute sets of measure zero that are not relevant for the variational formulation.

If we consider all the points $\mathbf{x}$ on several different faces Γ_{k_j}, $j = 1, \ldots, \nu$, then their common outflow directions are contained in the intersection of the outflow hemispheres of the faces. We denote these unique common outflow regions by

$$S_q := \bigcap_{k=k_1,\ldots,k_\nu} \Sigma_k, \ q = 1, \ldots, n_S,$$
$$\text{such that } S_q \neq \emptyset \wedge (q \neq r \Rightarrow S_q \cap S_r = \emptyset).$$

As the regions S_q are bounded by great circles on the sphere $\mathcal{S}^2$, they are spherical polygons. For $d_\mathcal{S} = 1$, the regions represent intervals of the circle. On the S_q, we define additional angular basis functions $S_{n,m}^{(d_\mathcal{S},q)}$, which for our examples with $d_\mathcal{S} = 1$ are dilated Legendre polynomials as defined in (38).

The span of these functions is denoted by

$$\mathbb{P}_l^{d_\mathcal{S},q} := \operatorname{span}\{S_{n,m}^{(d_\mathcal{S},q)} : n = 0, \ldots, l; \ m = 1, \ldots, m_{n,d_\mathcal{S}}\}. \tag{72}$$

Detail spaces on the spherical regions are defined as

$$W_{\mathcal{S},q}^l := \operatorname{span}\{S_{n,m}^{(d_\mathcal{S},q)} : n = l; \ m = 1, \ldots, m_{n,d_\mathcal{S}}\}. \tag{73}$$

When the angular region S_q is given, we denote the region of the physical domain boundary from which we obtain outflow into S_q by

$$\Gamma_+(S_q) := \{\mathbf{x} \in \partial D : \mathbf{n}(\mathbf{x}) \cdot \mathbf{s} > 0 \ \forall \mathbf{s} \in S_q\}. \tag{74}$$

For the setup of the sparse tensor product search space $\hat{V}_0^{L,N}$ with boundary conditions, we split the nested function space on the physical domain into several spaces:

$$V_D^l = V_{D,0}^l \oplus \sum_{q=1}^{n_S} V_{\partial D,q}^l, \tag{75}$$

in which $V_{D,0}^l$ contains the functions which are zero on the boundary,

$$V_{D,0}^l := \{v \in V_D^l : v|_{\partial D} = 0\}, \tag{76}$$

and $V_{\partial D,q}^l$ contains the functions of which the non-zero boundary part is completely contained in $\Gamma_+(S_q)$:

$$V_{\partial D,q}^l := \{\alpha \in V_D^l : \alpha(\mathbf{x}) = 0 \ \forall \mathbf{x} \in \partial D \setminus \Gamma_+(S_q)\}. \tag{77}$$

This means that some physical basis functions can be contained in several $V^l_{\partial D,q}$ with different q.

The same separation is possible for the detail spaces W^l_D into $W^l_{D,0}$ and $W^l_{\partial D,q}$. Then we can define the full tensor product space with boundary conditions $V_0^{L,N}$ as

$$V_0^{L,N} := \left(V^L_{D,0} \otimes \mathbb{P}_N^{d_\mathcal{S}}\right) \oplus \bigoplus_{q=1}^{n_S} \left(V^L_{\partial D,q} \otimes \mathbb{P}_N^{d_\mathcal{S},q}\right) \tag{78}$$

$$= \bigoplus_{\substack{0\le l_D\le L\\ 0\le l_S\le N}} W^{l_D}_{D,0} \otimes W^{l_S}_{\mathcal{S}} \oplus \bigoplus_{q=1}^{n_S} \bigoplus_{\substack{0\le l_D\le L\\ 0\le l_S\le N}} W^{l_D}_{\partial D,q} \otimes W^{l_S}_{\mathcal{S},q}, \tag{79}$$

The sparse version of the tensor product space is then defined as

$$\hat{V}_0^{L,N} := \left(V^L_{D,0} \hat{\otimes} \mathbb{P}_N^{d_\mathcal{S}}\right) \oplus \bigoplus_{q=1}^{n_S} \left(V^L_{\partial D,q} \hat{\otimes} \mathbb{P}_N^{d_\mathcal{S},q}\right) \tag{80}$$

$$= \bigoplus_{0\le f(l_D,l_S)\le L} W^{l_D}_{D,0} \otimes W^{l_S}_{\mathcal{S}} \oplus \bigoplus_{q=1}^{n_S} \bigoplus_{0\le f(l_D,l_S)\le L} W^{l_D}_{\partial D,q} \otimes W^{l_S}_{\mathcal{S},q}. \tag{81}$$

To illustrate these tensorizations, we describe and distinguish between several cases depending on the basis function α_i (see also Fig. 2):

1. If $\alpha_i(\mathbf{x})$ is non-zero only on the interior of D and zero on all Γ_k, the only product combinations need to be those with full sphere harmonics. Combinations with angular region functions are not required.

2. If $\alpha_i(\mathbf{x})$ is non-zero on several faces $\Gamma_{k_1}, \ldots, \Gamma_{k_\nu}$, only combinations with angular region functions $S^{(d_\mathcal{S},q)}_{n,m}(\mathbf{s})$ which are non-zero on the spherical regions S_q that are in the intersection of all outflow hemispheres $\Sigma_{k_1}, \ldots, \Sigma_{k_\nu}$ are conforming. Special cases are:

   a) $\alpha_i(\mathbf{x})$ is non-zero only on one Γ_k. Then only combinations with angular region functions that are non-zero on the hemisphere Σ_k are conforming.

   b) $\alpha_i(\mathbf{x})$ is non-zero on several faces $\Gamma_{k_1}, \ldots, \Gamma_{k_\nu}$ of which the unit normals $\mathbf{n}_{k_1}, \ldots, \mathbf{n}_{k_\nu}$ do not point into a common hemisphere, i. e. $\cap_{k=k_1,\ldots,k_\nu} \Sigma_k = \emptyset$. Then any combination involving $\alpha_i(\mathbf{x})$ cannot be contained in the tensor product spaces since there is no common outflow direction of the faces.

The number of angular basis functions to choose from for a product basis function increases from $M_\mathcal{S}$ to $M_{\mathcal{S},\text{tot}} := (n_S + 1)M_\mathcal{S}$, the number of physical basis functions stays at M_D. The total number of degrees of freedom of $\hat{V}_0^{L,N}$ or $V_0^{L,N}$, respectively, increases depending on the dimensionality and geometry of the problem, but the increase is subasymptotic in L, i. e. the ratio of boundary functions to interior functions goes to zero if the physical resolution is increased (for the structure of the function spaces and contained degrees of freedom see also Fig. 3).

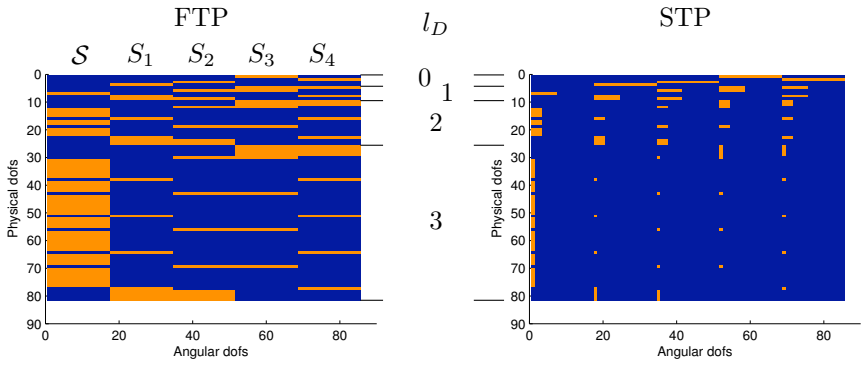

Figure 3: Marked degrees of freedom are conforming and included in the full tensor (left, 1853 dofs) or sparse tensor (right, 275 dofs) product space, respectively. Leftmost column contains combinations with full-sphere harmonics, following columns those with Legendre polynomials over spherical regions S_q.

Remark 2. A formal derivation of an estimate for the sparse tensor product space with boundary conditions has not been obtained yet. However, the numerical experiments in Section 4 suggest that estimates analogous to those for the case without boundary conditions in Section 3.2 are valid for the case with boundary conditions.

4 Numerical experiments

In order to test the theoretical convergence estimates from Thms. 3.3 and 3.4 in cases with boundary conditions we conduct a number of numerical experiments.

4.1 Algorithm

Our method has been implemented in an algorithm in MATLAB which has not been optimized for performance yet.

First, we calculate the physical and angular stiffness matrices separately by quadrature of the integrals over the physical and angular domain that arise out of the separation of the bilinear form (10) into physical and angular part. For the quadrature in D, we use a Gauss-Legendre rule in 2D which integrates the terms of the bilinear form involving product combinations of linear physical basis functions exactly up to rounding errors if the absorption coefficient $\kappa(\boldsymbol{x})$ is constant. The quadrature in the angular domain is performed by the trapezoidal rule for product combinations of the periodic harmonic functions on the full circle and by a Gauss-Legendre rule for combinations involving at least one Legendre polynomial of an angular region. The number of sample points of the quadrature rules is chosen such that we obtain accuracy up to rounding errors for pure harmonic combinations and a relative integration error tolerance of 10^{-13} for combinations over angular regions, as some of the terms in the bilinear form include mixed combinations of trigonometric functions and Legendre polynomials which are not solved exactly by Gauss-Legendre quadrature.

Entries of the load vector are calculated using the same quadrature rules. For test cases with a prescribed separable solution $u(\boldsymbol{x}, \boldsymbol{s}) = U(\boldsymbol{x})Y(\boldsymbol{s})$, we compute these entries by integration of the bilinear form (10) with solution $u(\mathbf{x}, \mathbf{s})$ and basis functions inserted while exploiting separability. For applications with given right hand side function $I_b(\boldsymbol{x})$, we evaluate the load functional (11). In both cases, iterative increase of quadrature nodes leads to a relative integration error tolerance of 10^{-13}.

The linear system is solved by a Conjugate Gradient method without preconditioning. Matrix-vector-multiplication is done in two steps: The matrix of all possible degrees of freedom is multiplied with the physical stiffness matrix producing some fill-in in the non-active parts of the intermediate degrees of freedom matrix. The intermediate matrix is then multiplied with the angular stiffness matrix. In the result, non-active degrees of freedom are truncated. We terminate the Conjugate Gradient method if the ℓ^2-norm of the dof (degrees of freedom) residual vector is less than 10^{-20}.

4.2 Quantities of interest

As the radiative intensity is a function of several variables, we are going to inspect derived quantities of reduced dimensionality to simplify visualization. Such quantities are the incident radiation $G(\boldsymbol{x})$, the heat flux $\boldsymbol{q}(\boldsymbol{x})$, and the net emission $\nabla \cdot \boldsymbol{q}(\boldsymbol{x})$,

which are defined and related by

$$G(\boldsymbol{x}) = \int_{\mathcal{S}^{d_S}} u(\boldsymbol{x}, \boldsymbol{s}) \mathrm{d}\boldsymbol{s} \tag{82}$$

$$\boldsymbol{q}(\boldsymbol{x}) = \int_{\mathcal{S}^{d_S}} u(\boldsymbol{x}, \boldsymbol{s}) \boldsymbol{s} \mathrm{d}\boldsymbol{s} \tag{83}$$

$$\nabla \cdot \boldsymbol{q}(\boldsymbol{x}) = \kappa(\boldsymbol{x})(\begin{Bmatrix} 4\pi & \text{if } d_{\mathcal{S}} = 2 \\ 2\pi & \text{if } d_{\mathcal{S}} = 1 \end{Bmatrix} I_b(\boldsymbol{x}) - G(\boldsymbol{x})). \tag{84}$$

In simulations of high-temperature situations, the radiative intensity enters the calculations in the energy equation as the divergence of the heat flux (Modest 2003, ch. 1), hence the interest in the net emission.

In experiments with a prescribed solution $u(\boldsymbol{x}, \boldsymbol{s})$, we compute the relative error of the numerical solution $u_{L,N}(\boldsymbol{x}, \boldsymbol{s})$ by

$$err_X = \|u - u_{L,N}\|_X / \|u\|_X,$$

where X stands for one of the norms $L^2(D \times \mathcal{S}^{d_S})$, $H^{1,0}(D \times \mathcal{S}^{d_S})$, $A(D \times \mathcal{S}^{d_S})$, the last one defined in (14) as the energy norm. From considerations about the convergence properties in Sec. 3.2.2, we obtain upper limits for the convergence rates.

In applications without known solution, we compute a reference solution with the discrete ordinates (DO) method and use this solution to estimate the error in the incident radiation $G_{L,N}(\mathbf{x})$ of the numerical solution $u_{L,N}(\mathbf{x}, \mathbf{s})$. In the DO method, the angular domain is discretized into 256 directions, along which we calculate the solution by the method of lines and a standard non-stiff integrator in MATLAB. The line integrals are then interpolated to the FEM mesh in the physical domain corresponding to a resolution of $L = 7$. We compute the relative error in the incident radiation as

$$err(G_{L,N})_X = \|G - G_{L,N}\|_X / \|G\|_X,$$

where G is the reference solution of the incident radiation and X stands for the $L^2(D)$- or $H^1(D)$-norm, respectively.

4.3 Experiments

All experiments have been conducted on the physical domain $D = [0, 1]^2$, the unit square, with zero inflow boundary conditions. The absorption coefficient function is constant $\kappa(\boldsymbol{x}) = 1$. For our basis we use hierarchical hat functions on a square mesh with mesh size $h = 2^{-L}$ in the physical domain. In the angular domain, harmonics in 1D are employed for full circle basis functions and Legendre polynomials for basis functions on the quarter circle angular regions.

In order to isolate the convergence rates over the domains D and $\mathcal{S}^{d_S}$ and to test the estimates (56) and (69) in the case with boundary conditions, we refine in physical resolution only by incrementing L by 1 and fixing the angular order or vice versa, then N is doubled in each refinement step and L is constant. However, in normal operation

one would rather use the equilibration relation (57) to increase the resolution in D and $\mathcal{S}^{ds}$ in a combined manner. Experiments 5 and 6 are examples for combined refinement.

4.3.1 Experiment 1

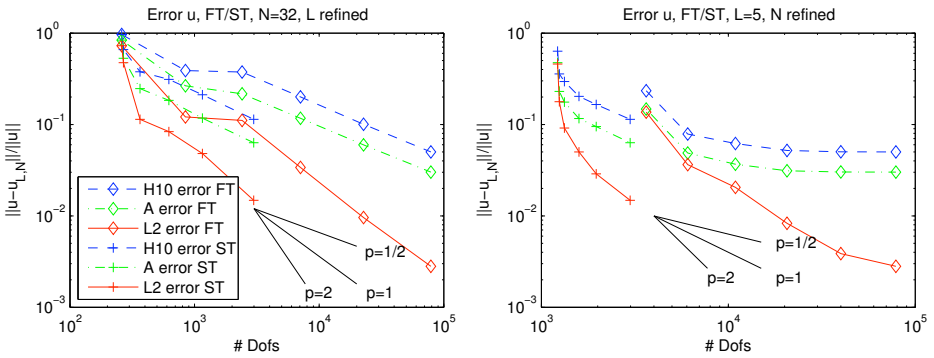

Figure 4: Experiment 1: Convergence of numerical solution $u_{L,N}$ to prescribed solution u for $L = 0, 1, \ldots, 5$ (left) or $N = 1, 2, 4, \ldots, 32$ (right).

In this experiment, we prescribe a polynomial of degree 3 in x_1 and degree 4 in x_2, non-vanishing on one side of the boundary, and a triangle function in the outflow direction:

$$u(\boldsymbol{x}, \varphi) = (-1(x_1 - 1)^2 + 1)(-4(x_2 - 1/2)^2 + 1)x_1 x_2(-4(x_2 - 1)) \cdot \begin{cases} \frac{-2}{\pi}\varphi + 1 & \text{if } 0 \le \varphi < \frac{\pi}{2}, \\ \frac{2}{\pi}(\varphi - \frac{3\pi}{2}) & \text{if } \frac{3\pi}{2} < \varphi < 2\pi, \\ 0 & \text{else.} \end{cases}$$

Here we find the situation that the angular resolution (order N) is sufficiently large to obtain the convergence rate for physical refinement expected from Thms. 3.3 and 3.4. In Fig. 4 on the left, the order of the convergence in the L^2-error is about 1, for the $H^{1,0}$-error and A-error about 1/2 as predicted by the error estimate (56) with $d = 2$ and $s = 1$. Furthermore, the ST method achieves a smaller error than the FT method for setups with similar numbers of degrees of freedom. In the right plot of Fig. 4, we see that for smaller numbers of degrees of freedom we obtain rapid convergence which, however, comes to a halt at higher numbers of dofs because the combined error is limited by the maximum contribution from angular and physical domain.

4.3.2 Experiment 2

For this test case we prescribe the same polynomial as in the previous experiment but replace the angular part of the solution by a function discontinuous at the $\varphi = 2\pi$ to

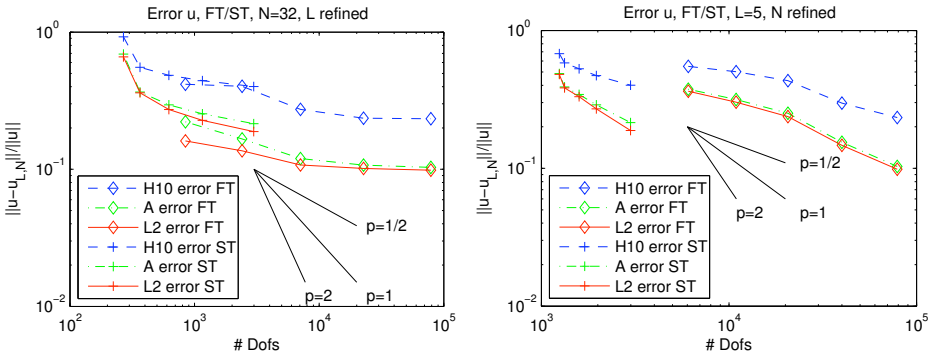

Figure 5: Experiment 2: Convergence of numerical solution $u_{L,N}$ to prescribed solution u for $L = 1, \ldots, 5$ (left) or $N = 2, 4, \ldots, 32$ (right).

$\varphi = 0$ transition:

$$u(\boldsymbol{x}, \varphi) = (-1(x_1 - 1)^2 + 1)(-4(x_2 - 1/2)^2 + 1)x_1 x_2(-4(x_2 - 1)) \cdot \begin{cases} \left(\frac{\sin(8\varphi)}{8\varphi}\right)^2 & \text{if } 0 \le \varphi < \frac{\pi}{2}, \\ 0 & \text{else.} \end{cases}$$

Here the convergence situation is reversed. The right plot in Fig. 5 shows a low convergence rate of about 1/2 for the $H^{1,0}$-error for angular refinement, which is due to the angular discontinuity in the solution. Obviously the discontinuity cannot be captured by the harmonics, a wavelet discretization could achieve higher convergence rates. Physical refinement is only effective for very small L, as can be seen from the left part of Fig. 5. Above a certain point, the limiting contribution to the error comes from the angular domain. In the effective angular refinement, the ST method surpasses the FT method with the same error at fewer dofs.

4.3.3 Experiment 3

We remove the angular discontinuity by extending the angular part of the prescribed solution with its mirrored image for $\frac{3\pi}{2} < \varphi < 2\pi$:

$$u(\boldsymbol{x}, \varphi) = (-1(x_1 - 1)^2 + 1)(-4(x_2 - 1/2)^2 + 1)x_1 x_2(-4(x_2 - 1)) \cdot \begin{cases} \left(\frac{\sin(8\varphi)}{8\varphi}\right)^2 & \text{if } 0 \le \varphi < \frac{\pi}{2}, \\ \left(\frac{\sin(8(2\pi-\varphi))}{8(2\pi-\varphi)}\right)^2 & \text{if } \frac{3\pi}{2} < \varphi < 2\pi, \\ 0 & \text{else.} \end{cases}$$

In this example, the spectral discretization in angle can leverage its full potential since the solution is completely smooth. In effect, in the full tensor method the numerical solution converges super-algebraically (see Fig. 6 right) until the oscillations

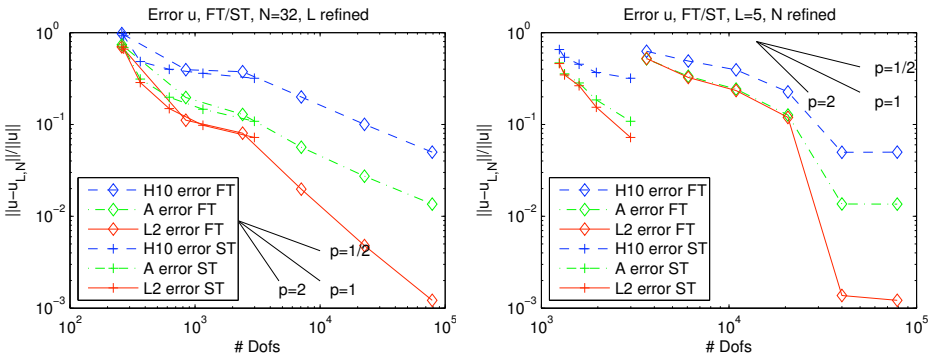

Figure 6: Experiment 3: Convergence of numerical solution $u_{L,N}$ to prescribed solution u for $L = 0, 1, \ldots, 5$ (left) or $N = 1, 2, 4, \ldots, 32$ (right).

of the angular solution can be fully captured at $N = 16$, further refinement in angle doesn't reduce the error any further. For physical refinement we obtain the maximum rate $1/2$ in the $H^{1,0}$-error as in the first experiment. The ST method yields a rate of $1/2$ in angular refinement but has a better ratio of error per employed dofs, in physical refinement the curves of FT and ST methods almost overlie each other to give the same rates and ratios.

4.3.4 Experiment 4

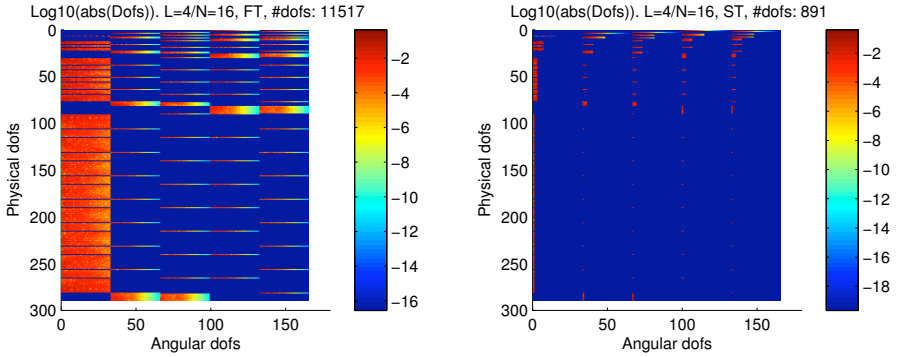

Figure 7: Experiment 4: Magnitude of active degrees of freedom (left FT, right ST). First column corresponds to inner dofs, then each of the following four columns contains dofs of boundary basis functions which are non-zero on one of the four faces of D.

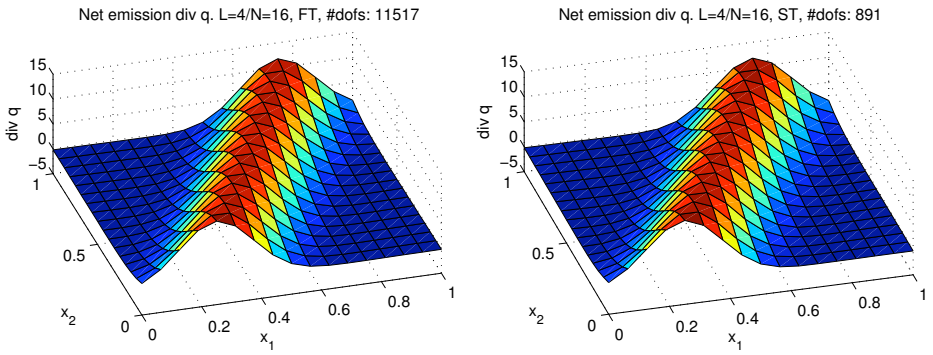

Figure 8: Experiment 4: Net emission (left FT, right ST).

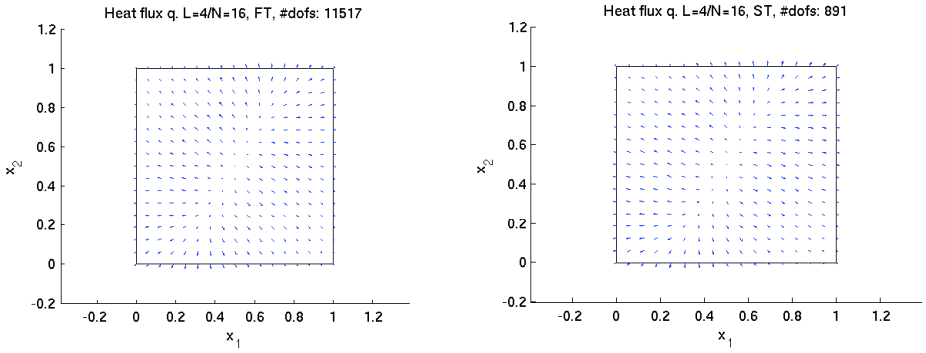

Figure 9: Experiment 4: Heat flux (left FT, right ST).

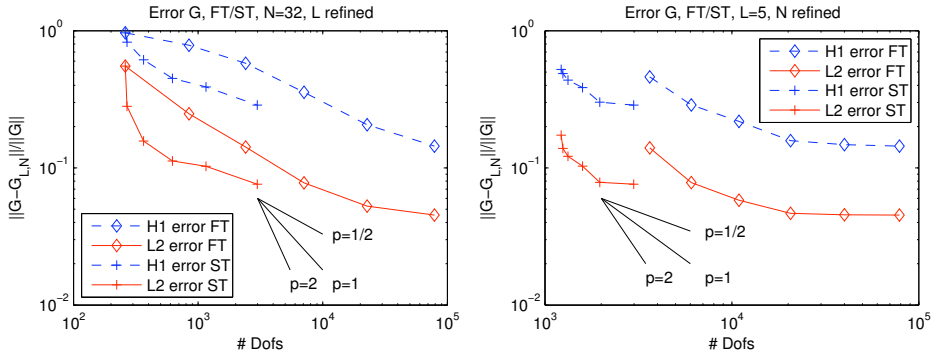

Figure 10: Experiment 4: Convergence in incident radiation (Eq. 82) of numerical solution $G_{L,N}$ to reference solution G for $L = 0, 1, \ldots, 5$ (left) or $N = 1, 2, 4, \ldots, 32$ (right).

This example is an application with a degenerate Gaussian on the right hand side:

$$I_b(\boldsymbol{x}) = \exp\left(-8(\boldsymbol{x} - \begin{pmatrix}0.5\\0.5\end{pmatrix})^\top \begin{pmatrix}4 & -2\\-2 & 1\end{pmatrix}(\boldsymbol{x} - \begin{pmatrix}0.5\\0.5\end{pmatrix})\right).$$

We observe that the magnitude of the degrees of freedom clearly drops off for angular basis functions of higher index, especially in the angular regions where Legendre polynomials are used (see Fig. 7).

Fig. 8 compares the net emission and Fig. 9 the heat flux of the FT and ST solutions. The solutions are qualitatively identical, even though the FT version uses 11517 degrees of freedom and the ST version only 891.

Convergence orders for the error of the incident radiation are 1/2 for the H^1-error and between 1 and 1/2 for the L^2-error for physical refinement (Fig. 10 left). Angular refinement achieves convergence orders of about 1 for both errors for smaller number of dofs, but then convergence slows down for higher number of dofs, which means that the error is again physically limited here (Fig. 10 right). For L- and N-refinement, the ST method outperforms the FT method in terms of error per number of dofs.

4.3.5 Experiment 5

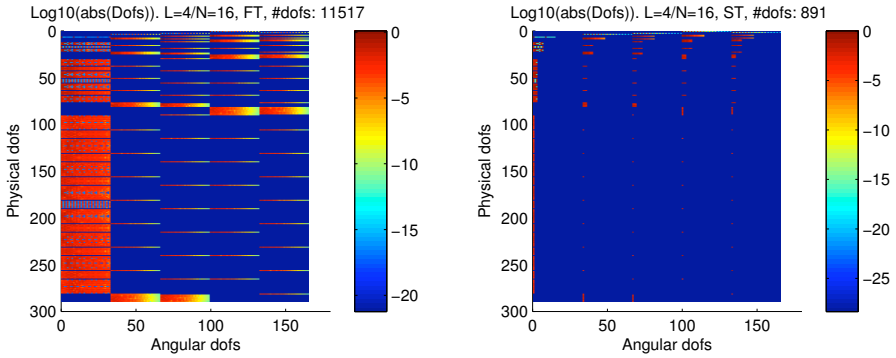

Figure 11: Experiment 5: Magnitude of active degrees of freedom (left FT, right ST).

Here we use a $C^\infty(D)$ bump function, smooth and compactly supported, on the right hand side:

$$I_b(\boldsymbol{x}) = \begin{cases} 10^4 \exp\left(\frac{-1}{0.25-(x_1-0.5)^2} + \frac{-1}{0.25-(x_2-0.5)^2}\right) & \text{if } 0.25 < x_1, x_2 < 0.75, \\ 0 & \text{else.} \end{cases}$$

The plot of the magnitude of the degrees of freedom for the FT case (Fig. 11 left) reveals that the interior degrees of freedom (left column) do not drop off very fast. As a consequence, the incident radiation shown in Fig. 12 differs slightly between the FT and the ST case for identical L and N. Therefore the error estimate for the incident

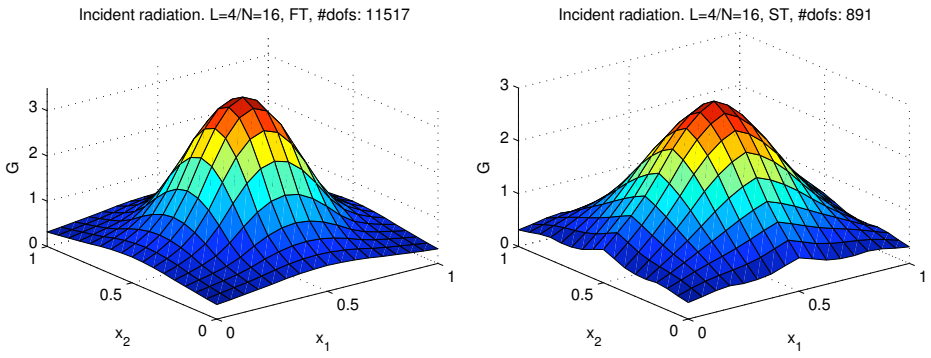

Figure 12: Experiment 5: Incident radiation (left FT, right ST).

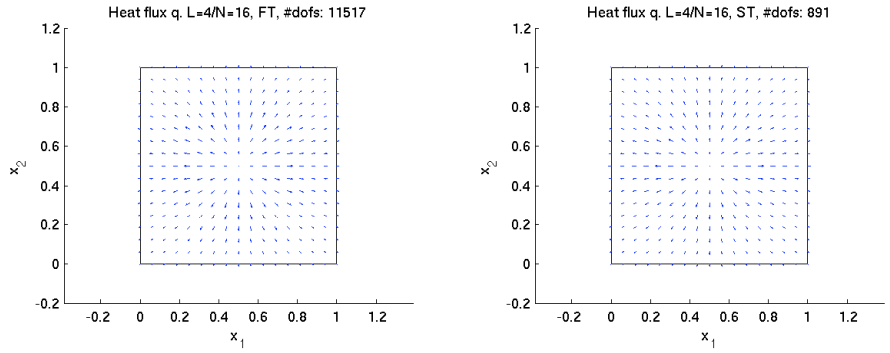

Figure 13: Experiment 5: Heat flux (left FT, right ST).

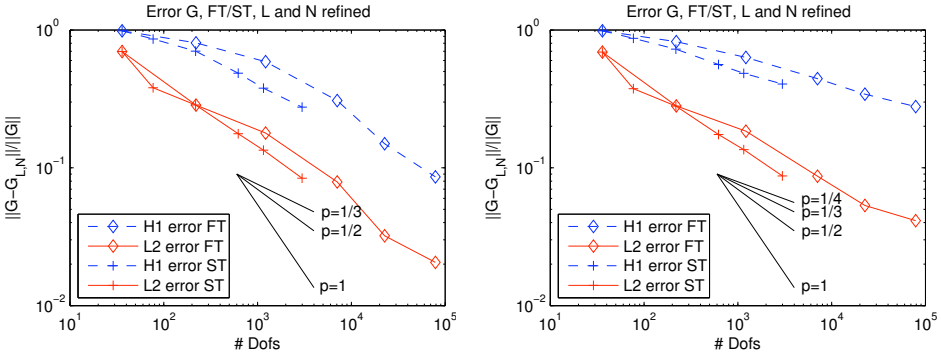

Figure 14: Experiments 5 (left) and 6 (right): Error in incident radiation for $L = 0, 1, \ldots, 5$ and $N = \min\{2^{L+2}, 32\}$.

radiation is worse in the ST case when L and N are the same (see Fig. 14 left), but note that the ST product method employs far fewer degrees of freedom. When setups with similar numbers of degrees of freedom are compared, the ST product method has an edge over the FT product method. The convergence rate in the H^1-error of the incident radiation is almost $1/2$ for combined refinement of the physical and angular resolution when N is chosen to be $N = \min\{2^{L+2}, 32\}$.

4.3.6 Experiment 6

In this experiment, the blackbody intensity is one on a circle in the physical domain:

$$I_b(\boldsymbol{x}) = \begin{cases} 1 & \text{if } (x_1 - 0.5)^2 + (x_2 - 0.5)^2 < \frac{1}{4^2}, \\ 0 & \text{else.} \end{cases}$$

The right hand side function $I_b(\boldsymbol{x})$ is therefore compactly supported and discontinuous. The discontinuity causes the convergence rate for combined refinement to drop to about $1/4$ in the H^1-error (see Fig. 14 right), when $N = \min\{2^{L+2}, 32\}$ as before. For setups with the same number of degrees of freedom, the ST method again results in a smaller error than the FT method.

5 Conclusion

We have shown that the advantages of sparse tensorization presented by Widmer et al. (2007) for wavelet discretization of the angular domain can also be harnessed for a spectral discretization with spherical harmonics in the radiative transfer problem. The sparse tensor approach is not limited to polynomial discretizations in angle. Error estimates in the spectral discretization for the problem neglecting boundary conditions can be derived in a fashion analogous to the estimates in the wavelet discretization. To treat the problem with zero Dirichlet boundary conditions in the framework of sparse tensorization, we split the physical function space into boundary and non-boundary subspaces and tensorize them with conforming angular function spaces.

Numerical experiments have confirmed that the estimated convergence rates of $M_D^{-1/2}$ for the $H^{1,0}$-error in two physical dimensions with piecewise linear physical basis functions can be achieved for refinement of the physical resolution, where M_D is the number of degrees of freedom in physical space. Likewise, the experiments have demonstrated that convergence in the angular domain can be superalgebraical if the solution is sufficiently smooth, but reduces to rates of $M_{\mathcal{S}}^{-1}$ or less if discontinuities occur in the angular part of the solution. $M_{\mathcal{S}}$ is the number of degrees of freedom in the angular space. In every conducted experiment, the sparse tensor product method has given a better error per employed number of degrees of freedom ratio than the full tensor product method.

References

Miguel A. Blanco, M. Flórez, and M. Bermejo. Evaluation of the rotation matrices in the basis of real spherical harmonics. *Journal of Molecular Structure (Theochem)*, 419:19–27, 1997.

Hans-Joachim Bungartz and Michael Griebel. Sparse grids. In Arieh Iserles, editor, *Acta numerica*, volume 13, pages 147–269. Cambridge University Press, 2004.

Martin Frank. Approximate models for radiative transfer. *Bull. Inst. Math. Acad. Sinica (New Series)*, 2:409–432, 2007.

M. Griebel, P. Oswald, and T. Schiekofer. Sparse grids for boundary integral equations. *Numer. Math.*, 83(2):279–312, 1999.

Claes Johnson. *Numerical Solution of Partial Differential Equations by the Finite Element Method*. Cambridge University Press, Cambridge, 1987.

Guido Kanschat. *Parallel and adaptive Galerkin methods for radiative transfer problems*. PhD thesis, University of Heidelberg, 1996. URL `http://archiv.ub.uni-heidelberg.de/volltextserver/volltexte/2006/6331/`.

Guido Kanschat, Wilhelm von Waldenfels, Christian Y. Cardall, Stephen Wright, Simon Arridge, Martin Schweiger, Erik Meinköhn, Maarten Baes, A. Hujeirat,

Eugene H. Avrett, Jiří Kubát, Daniela Korčáková, Wolfgang Kalkofen, Dimitris Stamatellos, Anthony P. Whitworth, Avery Meiksin, Sabine Richling, Dmitrij Semionov, Vladas Vansevičius, and Oliver Dorn. *Numerical Methods in Multidimensional Radiative Transfer*. Springer, 2008. doi: 10.1007/978-3-540-85369-5.

Edward W. Larsen, Guido Thömmes, Axel Klar, Mohammed Seaïd, and Thomas Götz. Simplified P_N approximations to the equations of radiative heat transfer and applications. *Journal of Computational Physics*, 183(2):652 – 675, 2002. ISSN 0021-9991. doi: 10.1006/jcph.2002.7210.

Thomas A. Manteuffel, Klaus J. Ressel, and Gerhard Starke. A boundary functional for the least-squares finite-element solution of neutron transport problems. *SIAM Journal on Numerical Analysis*, 37(2):556–586, 2000. doi: 10.1137/S0036142998344706.

Solomon G. Mikhlin and Siegfried Prössdorf. *Singular Integral Operators*. Springer, 1986.

Michael F. Modest. *Radiative Heat Transfer*. Elsevier, 2nd edition, 2003.

Michael F. Modest and Jun Yang. Elliptic PDE formulation and boundary conditions of the spherical harmonics method of arbitrary order for general three-dimensional geometries. *Journal of Quantitative Spectroscopy & Radiative Transfer*, 109:1641–1666, 2008. doi: 10.1016/j.jqsrt.2007.12.018.

Hoang Nguyen. *Finite element wavelets for solving partial differential equations*. PhD thesis, University of Utrecht, 2005. URL `http://igitur-archive.library.uu.nl/dissertations/2005-0504-200310/index.htm`.

Hans Triebel. *Interpolation theory, function spaces, differential operators*. Barth, Heidelberg, 2nd edition, 1995.

Tobias von Petersdorff and Christoph Schwab. Numerical solution of parabolic equations in high dimensions. *M2AN Math. Model. Numer. Anal.*, 38(1):93–127, 2004. doi: 10.1051/m2an:2004005.

G. Widmer, R. Hiptmair, and Ch. Schwab. Sparse adaptive finite elements for radiative transfer. *Journal of Computational Physics*, 227:6071–6105, 2008. doi: 10.1016/j.jcp.2008.02.025.

Gisela Widmer. *Sparse Finite Elements for Radiative Transfer*. PhD thesis, ETH Zürich, 2009. URL `http://e-collection.ethbib.ethz.ch/view/eth:374`. No. 18420.

Gisela Widmer, R. Hiptmair, and Ch. Schwab. Sparse adaptive finite elements for radiative transfer. Technical Report 01, SAM, ETH Zürich, January 2007. URL `http://www.sam.math.ethz.ch/reports/2007/01`.

Research Reports

No.	Authors/Title
10-33	*K. Grella and C. Schwab* Sparse tensor spherical harmonics approximation in radiative transfer
10-32	*P. Kauf, M. Torrilhon and M. Junk* Scale-induced closure for approximations of kinetic equations
10-31	*M. Hansen* On tensor products of quasi-Banach spaces
10-30	*P. Corti* Stable numerical scheme for the magnetic induction equation with Hall effect
10-29	*H. Kumar* Finite volume methods for the two-fluid MHD equations
10-28	*S. Kurz and H. Heumann* Transmission conditions in pre-metric electrodynamics
10-27	*F.G. Fuchs, A.D. McMurry, S. Mishra and K. Waagan* Well-balanced high resolution finite volume schemes for the simulation of wave propagation in three-dimensional non-isothermal stratified magneto-atmospheres
10-26	*U.S. Fjordholm, S. Mishra and E. Tadmor* Well-balanced, energy stable schemes for the shallow water equations with varying topography
10-25	*U.S. Fjordholm and S. Mishra* Accurate numerical discretizations of non-conservative hyperbolic systems
10-24	*S. Mishra and Ch. Schwab* Sparse tensor multi-level Monte Carlo finite volume methods for hyperbolic conservation laws with random intitial data
10-23	*J. Li, J. Xie and J. Zou* An adaptive finite element method for distributed heat flux reconstruction
10-22	*D. Kressner* Bivariate matrix functions
10-21	*C. Jerez-Hanckes and J.-C. Nédélec* Variational forms for the inverses of integral logarithmic operators over an interval